Industrial Crops & Products 197 (2023) 116657

Contents lists available at ScienceDirect

Industrial Crops & Products

journal homepage: www.elsevier.com/locate/indcrop

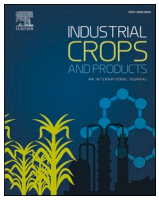

Integrated mRNA and miRNA omics reveal the regulatory role of UV-B radiation in active ingredient biosynthesis of *Chrysanthemum morifolium* Ramat

Yanjun Yang [a,b,1], Jie Liu [a,b,1], Taiyao Yi [a,b], Yao Li [a,b], Mengyuan Li [a,b], Haidi Liu [c], Lijun Zheng [a,b], Zhehao Chen [c], Juan Hao [a,b], Maojun Xu [a,b,*], Chenjia Shen [a,b,*]

[a] Zhejiang Provincial Key Laboratory for Genetic Improvement and Quality Control of Medicinal Plants, Hangzhou Normal University, Hangzhou, China
[b] Key Laboratory of Hangzhou City for Quality and Safety of Agricultural Products, College of Life and Environmental Sciences, Hangzhou Normal University, Hangzhou, China
[c] College of Life and Environmental Sciences, Hangzhou Normal University, Hangzhou, China

ARTICLE INFO

Keywords:
Bioactive ingredient
Chlorogenic acid
Differential expressed genes
Flavonoid
MicroRNA
Ultraviolet-B radiation

ABSTRACT

Ultraviolet-B (UV-B) is an effective elicitor that enhances bioactive ingredient biosynthesis in different plants. *Chrysanthemum morifolium* Ramat (C. *morifolium*) is a well-known herbal medicine and beverage material, which is cultivated in many Asian countries and regions. The C. *morifolium* inflorescences are the main accumulation sites for active ingredients, which include flavonoids and chlorogenic acid. However, the molecular mechanisms underlying UV-B-mediated bioactive ingredient biosynthesis in *C. morifolium* inflorescences remain largely unknown. High-throughput sequencing technologies have been applied to identify the messenger RNAs (mRNAs) and microRNAs (miRNAs) responsive to UV-B radiation in *C. morifolium* inflorescences. Many UV-B responsive genes are enriched in flavonoid, unsaturated fatty acid, phenylpropanoid, and carotenoid biosynthesis pathways. In this study, we identified 169 miRNAs belonging to 38 typical families were detected in our constructed libraries. In total, 1954 unigenes were predicted to be targets of 118 miRNAs. Six miRNAs, *PC-5p-7136_1319*, *PC-3p-78379_156*, *ath-MIR414-p5_2ss2CT21AC*, *PC-3p-154888_69*, *nta-miR171a_2ss8GT18GA* and *htu-miR403a* were involved in the regulation of active ingredient biosynthesis by targeting *4CL-like 5/9*, *CYP81E8*, *UGT91D1* and *UGT72B1* genes. Five miRNAs, *PC-5p-79_56613*, *ath-miR858a_L-1*, *ath-MIR414-p5_2ss15AC18AT*, *ath-MIR414-p5_2ss2CT21AC*, and *aly-miR393a-5p* were involved in regulation of flavonoid biosynthesis by targeting MYB-bHLH complex-related transcription factor genes. Our data provides a platform for identifying mRNAs and miRNAs involved in the UV-B-induced accumulation of bioactive ingredients in *C. morifolium* inflorescences.

1. Introduction

Chrysanthemum belongs to the Asteraceae family and is widely domesticated and cultivated in Southeast Asia (Su et al., 2019; Teixeira da Silva, 2003). As a major commercial cut flower, many *Chrysanthemum* species are used for gardening and landscaping (Anderson, 2006). In addition to their ornamental value, *Chrysanthemum morifolium* inflorescences are harvested for beverage and medicine utilizations (Yuan et al., 2020). *C. morifolium* inflorescences contain different phytochemicals, such as flavonoids, anthocyanins, and chlorogenic acid, which exert many medical effects, including antioxidant effects and preventing anti-inflammatory visceral injury (Lu et al., 2016). Consequently, commercial demand for *C. morifolium* inflorescences has increased year on year (Kazeroonian et al., 2018).

Plant secondary metabolism generates abundant active ingredients for human health, and is not only regulated by genetic factors but also environmental factors (Li et al., 2020; Zhan et al., 2022). Different environmental factors, including UV-B, latitude, extreme temperature and nitric oxide, function as effective elicitors to enhance active ingredient biosynthesis (Manivannan et al., 2016; Takshak and Agrawal,

* Corresponding authors at: Zhejiang Provincial Key Laboratory for Genetic Improvement and Quality Control of Medicinal Plants, Hangzhou Normal University, Hangzhou, China
E-mail addresses: xumaojunhz@163.com (M. Xu), shencj@hznu.edu.cn (C. Shen).
[1] These authors contributed equally to this work.

https://doi.org/10.1016/j.indcrop.2023.116657
Received 10 November 2022; Received in revised form 1 March 2023; Accepted 29 March 2023
Available online 1 April 2023

2016; Zheng et al., 2022). High UV-B radiation doses are negative factors involved in plant growth and productivity (Yao et al., 2013). However, phytochemical studies have revealed that low UV-B radiation doses exert beneficial effects during plant secondary metabolism (Chen et al., 2020). Recently, UV-B radiation was applied as a simple and environmentally-friendly method to enhance medicinal plant active ingredient biosynthesis (Hao et al., 2022; Jaiswal et al., 2022; Pandey et al., 2021). Low UV-B doses enhanced saponin accumulation, which is a major phytochemical compound in *Chlorophytum borivillianum* (Jaiswal et al., 2022). In the medicinal plant *Adhatoda vasica*, UV-B helped to facilitate oridonin oxide and α-bisabolol oxide-B biosynthesis (Pandey et al., 2021). Also, UV-B regulated active compound accumulation in *Dendrobium officinale* was confirmed by high performance liquid chromatography analysis (Chen et al., 2020). However, the regulatory function of UV-B radiation in active ingredient biosynthesis from *C. morifolium* inflorescences remain unclear.

Many transcriptomic analyses have identified secondary metabolism-related *C. morifolium* genes. CmTPS family genes were identified, with *CmTPS5* and *CmTPS8* encoding multi-product enzymes in monoterpenoid and sesquiterpenoid biosynthesis (Zhang et al., 2022). Whole-transcriptome analyses of mutant and normal *C. morifolium* capitula identified many transcription factors (TFs) related to anthocyanin biosynthesis (Liu et al., 2021a). Transcriptomic profiling revealed that down-regulation of *F-box* genes significantly increased diverse flavonoid levels (Jo et al., 2020). Comparative transcriptomic analyses revealed several TF genes, including *CmMYB305*, *CmMYB29*, *CmRAD3*, *CmbZIP61*, *CmAGL24*, and *CmNAC1*, that play important roles in carotenoid accumulation (Lu et al., 2019). Transcriptomic analysis of healthy and *Spodoptera litura*-infested *C. morifolium* plants identified 11 *TPS* candidates that were involved in herbivore-induced volatile terpene emission (Xu et al., 2021). A transcriptomic analysis of five cDNA libraries identified three *CmMYB* genes and one *CmbHLH* gene which were implicated in light-induced anthocyanin biosynthesis (Hong et al., 2015).

MicroRNAs are the most abundant class of endogenous noncoding small RNA molecules and play roles in the regulation of many plant biological processes (Dong et al., 2022). In *C. morifolium*, some TF family-related miRNAs have been identified and functionally analyzed. For example, a transcriptome-wide survey identified HD-ZIP, DOF, SBF-like, and Trihelix family-related miRNAs (Song et al., 2016a,b,c,d). MiRNA expression analyses identified several aphid-infestation-responsive *C. morifolium* miRNAs (Xia et al., 2015). Embryo-abortion-associated *Chrysanthemum* miRNAs and their targets were identified during a cross breeding process (Zhang et al., 2015). However, the secondary metabolism-related miRNAs remain largely unknown.

To reveal UV-B mediated regulatory complexity in *C. morifolium* secondary metabolism, integrated transcriptomic and miRNAomic analysis was performed. Using *C. morifolium* leaves, we previously identified many genes and miRNAs which were responsive to UV-B exposure (Yang et al., 2020; Yang et al., 2018). Although easy to harvest, leaves are not the main edible portion of *C. morifolium*. In the present study, inflorescences were harvested to reveal expression changes in active ingredient biosynthesis-related genes and miRNAs. Our data will give an opportunity to reveal the function of UV-B radiation in bioactive ingredient biosynthesis in *Chrysanthemum* plants.

2. Materials and methods

2.1. Plant materials and treatments

The *C. morifolium* cultivar '*Xiaoyangju*' was grown in a plantation at the 'Cangqian' campus, Hangzhou Normal University. Mature flowers from *C. morifolium* seedings were harvested and separated into four classes (three replicates in each class). The seedings in flowering stage were treated with UV-B radiation (10 μmol m^{-2} s^{-1}) for 0 h (CK), 3 h (U3), 6 h (U6), and 12 h (U12), respectively. Inflorescences were collected and frozen rapidly in liquid N_2 until used.

2.2. cDNA library construction

Total RNAs were extracted and purified using TRIzol reagent (Invitrogen, Shanghai, China) according to manufacturer's instructions. RNA quality was analyzed using an Agilent NanoDrop spectrophotometer (Santa Clara, CA, USA). A total of 10 mg RNAs were subjected to magnetic beads with oligo-dT (Thermo Fisher Scientific, Shanghai, China). RNA was cut into small fragments using divalent cations at elevated temperatures. RNA fragments were used for first strand cDNA synthesis using a cDNA preparation kit (Illumina, San Diego, CA, USA). Fragmentary RNAs were reverse-transcribed to create a cDNA library using an Illumina cDNA library construction kit (San Diego, USA). After purification, DNA fragments with sequencing adapters were generated using the Illumina Hiseq2500 platform according to its protocols (LC-Bio, Hangzhou, China) (Feng et al., 2023). Three repeats for each sample of mRNA sequencing were performed.

2.3. De novo assembly and gene annotation

Raw read quality was evaluated using in-house Perl scripts (LC-Bio, Hangzhou, China). Low quality reads were omitted and clean reads were assembled into contigs as previously described (Yang et al., 2018). Contig properties were calculated using Trinity software, and the longest sequences were selected as unigenes. The resulting sequences were searched against various databases for functional annotation. Using the *Arabidopsis* proteins as the query sequences, the homologous sequences of the *C. morifolium* inflorescences were searched by local BLASP program, with an *E*-value threshold of 10^{-10}.

2.4. Analysis of differentially expressed genes (DEGs)

The transcriptomes from all samples were used as a reference sequence for DEGs identification. Clean reads were mapped onto the reference sequence using Bowtie ver. 0.12.7 software. Genes with more than a two-fold change were selected as DEGs. Venn analysis was performed to identify the DEGs in different samples. GO and KEGG terms with a *P* value lower than 0.05 were assigned as DEGs.

2.5. Small RNA libraries construction and sequencing

Small RNA libraries preparation were carried out by LC-Bio (Hangzhou, China). About 1 μg of total RNAs from each sample were isolated to construct sRNA library. Briefly, the total RNAs were purified to produce sRNA fragments with lengths ranging from 18 to 30 nt. Then, the RNA fragments were ligated to the RNA sequencing adapter. cDNA libraries were generated by a reverse transcription reaction and PCR amplified. The PCR products were purified and processed by a HiSeq 2500 system (Illumina, San Diego, USA) according to the LC-Bio method. Three repeats for each sample of miRNA sequencing were performed.

2.6. Analysis of small RNA

The raw small RNA sequences were filtered to produce clean reads. All clean reads were searched against the GenBank (http://www.ncbi.nlm.nih.gov/genbank/) and Rfam 12.1 (https://xfam.wordpress.com) to annotate sRNAs and remove known non-coding RNAs (Yang et al., 2020, 2018). Protein-coding sequences were removed based on the *C. morifolium* reference transcriptome. The remaining sequences were used to predict miRNA secondary structure, and aligned to miRBase 21.0 to obtain the known miRNAs (Haunsberger et al., 2017). Novel miRNAs were predicted using miRDeep2 software (ver.2.0.5).

2.7. Analysis of differentially expressed miRNAs (DEMs)

The normalized expression value of different miRNA was calculated according to the Reads Per Kilobase Million method. DEGs and miRNAs (DEMs) between two sample groups were screened using the DESeq R package. The thresholds for a significant difference between sample groups were set as $P < 0.01$ and $|\log_2(\text{fold change})| > 1$. The expression patterns of DEMs across four groups were performed using the K-mean method.

2.8. Enrichment analysis of target genes

MiRNAs targets were predicted by psRobot and Target Finder using *C. morifolium* transcriptomic assembled sequence was used as a reference sequence (Sablok et al., 2019). The functional category analysis of miRNA target genes were performed using GO term and the KEGG pathway. The statistical significance of GO and KEGG enrichment analysis was measured by Fisher's exact test under the condition of a *P* value at 0.05.

2.9. Quantitative real-time PCR (qRT-PCR) analysis

A total of 3 μg RNAs were extracted and reverse transcribed to cDNA using ReverAid First Strand cDNA Synthesis Kit (Thermo Scientific, Shanghai, China). qRT-PCR was used to confirm the expression levels of several mRNAs according to our previous method (Yang et al., 2018). Three independent cDNA samples of each treatment group were used for the qRT-PCR validation. The *C. morifolium TUBB* gene was used as an internal standard.

2.10. Validation of DEMs

Stem-loop quantitative reverse transcription PCR was used to confirm the expression levels of several miRNAs according to our previous method (Yang et al., 2020). For qPCR analysis of miRNAs, *U6* gene was used as an internal standard.

2.11. Dual-luciferase report assay

To create effector constructs, the mature sequences of PC-5p-7136_1319 and aly-miR393a-5p were cloned into the pCAMBIA1301 vector. To create reporter constructs, the PC-5p-7136_1319 binding region of *4CL-like 9* and aly-miR393a-5p binding region of *bHLH62* (DN38440) were cloned into the pGreenII 0800-Luc vector. The dual-luciferase report experiment was used to confirm the relationship between miRNA and its target according to our previous method (Yang et al., 2020).

3. Results

3.1. Overview of C. morifolium transcriptomes

To identify *C. morifolium* responsive genes during UV-B exposure, expression profiles were analyzed. A total of 118.06 Gb of raw data was obtained, of which 107.55 Gb was valid data. After filtering, approximately 98.14% of clean reads reached the threshold score of Q20, and approximately 93.9% reached Q30 (Table S1). Pearson correlation between different sample groups (three repeats for each group) were shown in Fig. S1. Reads from the *C. morifolium* inflorescences were assembled using Trinity software (Fig. 1a-c). In detail, the minimum

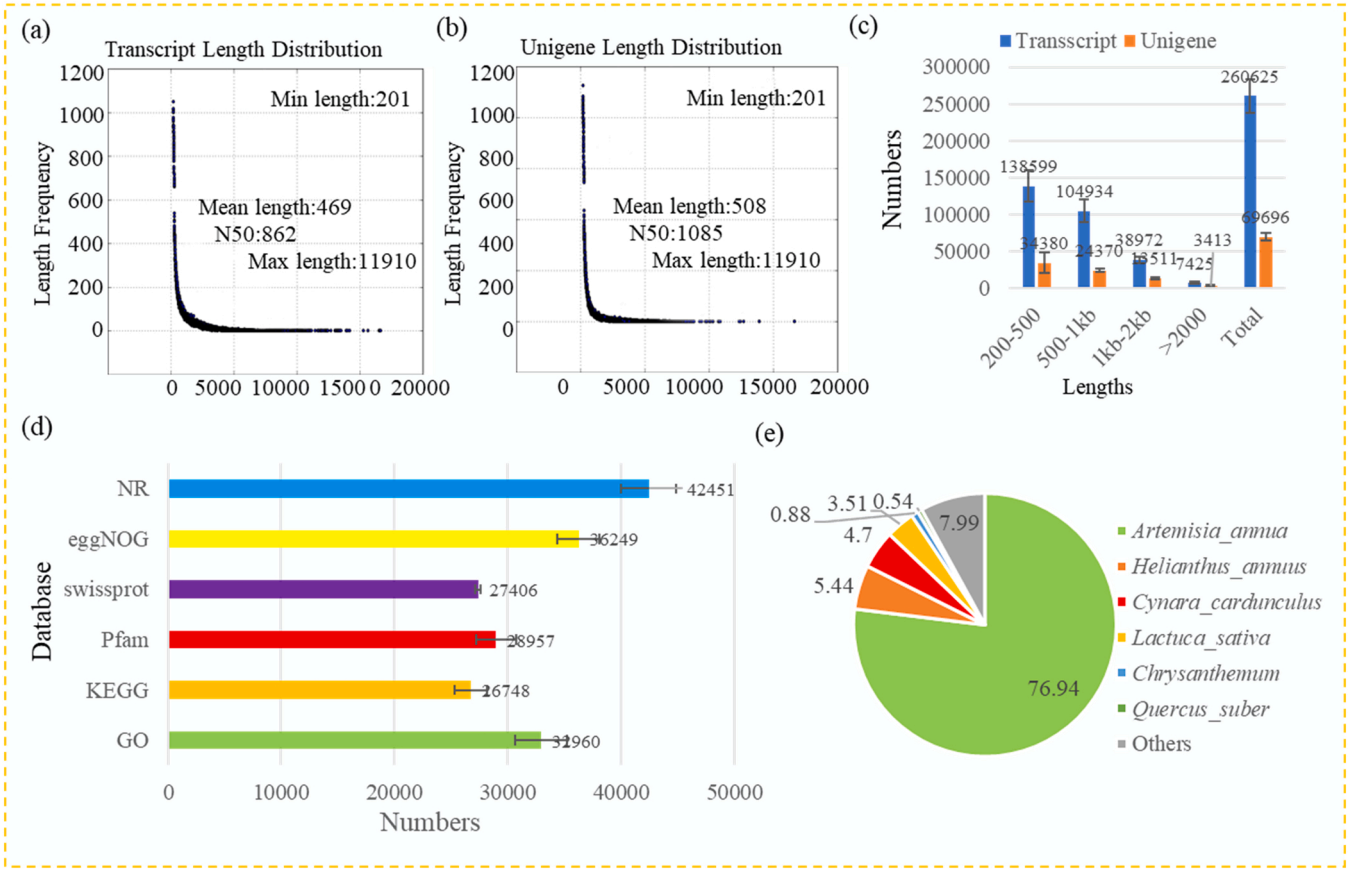

Fig. 1. Basic information for *C. morifolium* RNA sequencing. (a-b) Basic parameters of transcripts and unigenes of *C. morifolium*. (c) Length distribution of assembled transcripts and unigenes in *C. morifolium*. (d) Number of unigenes annotated by different databases, including Nr, eggNOG, Swissprot, Pfam, KEGG and GO databases. (e) Species distribution of all annotated unigenes. The numbers indicated the percentages of *C. morifolium* proteins similar to each public plant species.

length of transcripts and unigenes is 201 bp. The median lengths of transcripts and unigenes are 469 bp and 508 bp, respectively. A large number of genes were annotated in various protein databases (Fig. 1d). The largest number of unigenes were annotated in NR database (42,451 unigenes) and smallest number of unigenes were annotated in Swissprot database (27,406 unigenes). Annotation information suggested that most *C. morifolium* genes showed high similarity to *Artemisia annua*, *Helianthus annuus*, and *Cynara cardunculus* genes (Fig. 1e).

3.2. Analysis of differentially expressed genes (DEGs) under UV-B treatment

Many DEGs, including 1632 DEGs in the UV 3 h vs CK comparison, 2968 DEGs in the UV 6 h vs CK comparison, and 6438 DEGs in the UV 12 h vs CK comparison, were identified in different UV-B radiation treatment timepoints (Fig. 2a). Global gene expression profiles at different UV-B radiation timepoints are shown (Fig. 2b). Then, DEGs were grouped into different clusters. In detail, Cluster I included 1548 genes from the 6 h UV-B treatment group; Cluster III and VI included 3827 genes from 12 h UV-B treatment group; Cluster VII and VIII included 6791 genes significantly decreased during the UV-B treatment process; and Cluster III included 2547 genes significantly increased during UV-B treatment (Fig. 2c).

At 3 h, DEGs were significantly enriched in “temperature compensation of the circadian clock”, “cysteine-type peptidase activity”, and “circadian rhythm” gene ontology (GO) terms; at 6 h, the DEGs are significantly enriched in “quercetin 7-O-glucosyltransferase activity”, and “flavonoid glucuronidation” GO terms; and at 12 h, the DEGs are significantly enriched in “flavonoid biosynthetic process”, and “circadian rhythm” GO terms (Table S2-4).

3.3. Metabolic responses to UV-B radiation

The effects of UV-B treatments on *C. morifolium* inflorescence metabolisms were investigated. Significant *P* values for each primary and secondary metabolism-related Kyoto Encyclopedia of Genes and Genomes (KEGG) term was calculated. Metabolism-related KEGG terms were grouped into 11 classes and indicated by different color bars. Most significantly-changed KEGG terms belonged to flavonoid, lipid, phenylpropanoid, and pigment metabolism processes (Fig. 3a). For flavonoid metabolism, genes belonging to the “flavone and flavonol biosynthesis” and “flavonoid biosynthesis” terms were significantly changed after UV-B treatment. For lipid metabolism, genes belonging to the “biosynthesis of unsaturated fatty acids” term were significantly changed during the UV-B treatment process. For phenylpropanoid metabolism, the genes belonging to the “phenylpropanoid biosynthesis”

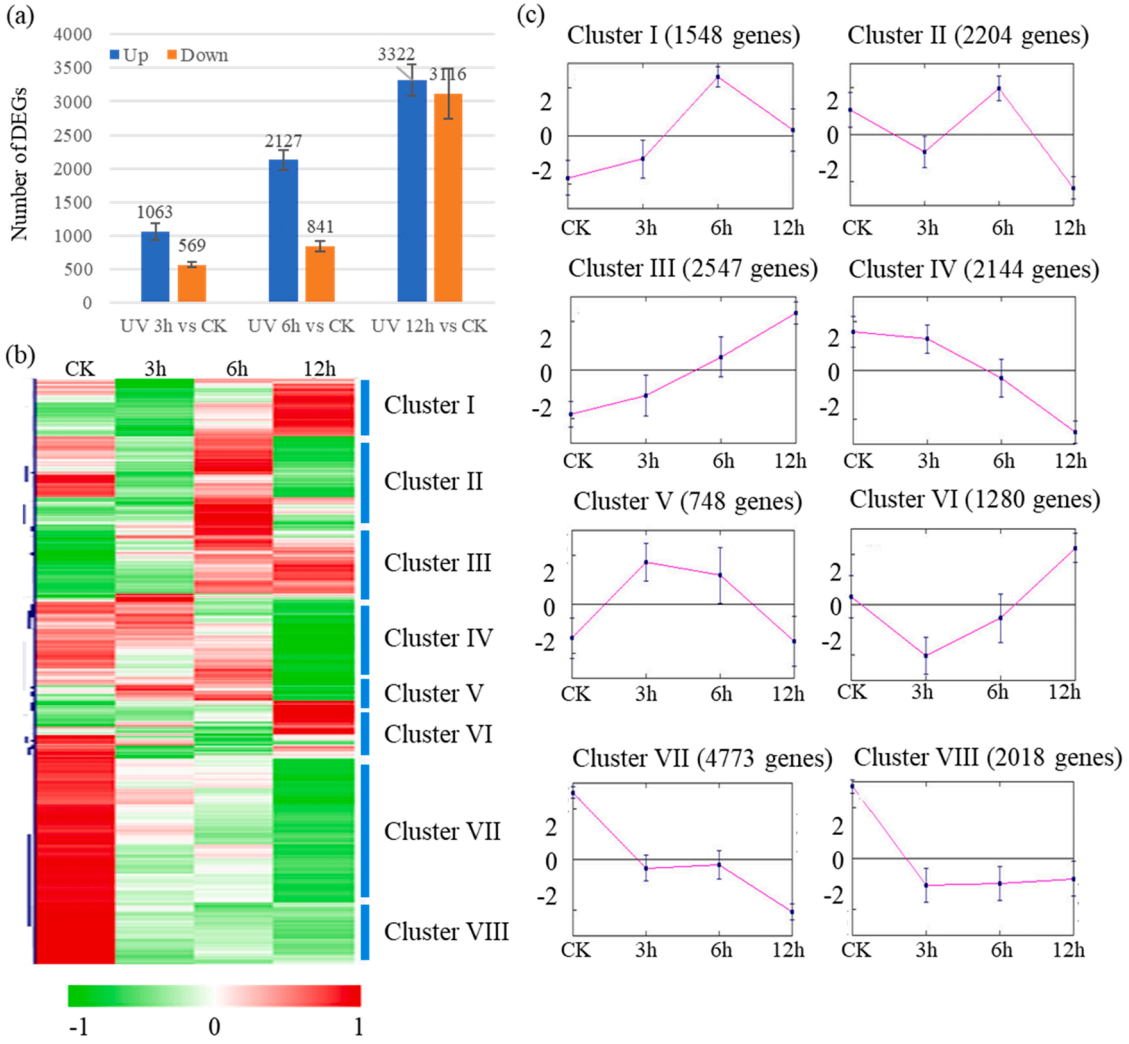

Fig. 2. Analysis of DEGs under UV-B radiation treatment in *C. morifolium*. (a) Number of up- and down- regulated unigenes in different companions. (b) Heat map for cluster analysis of DEGs by K-means method. The expression levels of each gene were normalized among four sample groups, including CK, 3 h, 6 h and 12 h. The red color indicated high expression level, green color indicated low expression level, and while color indicated median expression level. (c) MeV cluster analysis of differentially expressed genes from the gene expression profiles. The heatmap scale ranges from − 1 to + 1 on a $\log_2$ scale of normalized expression levels.

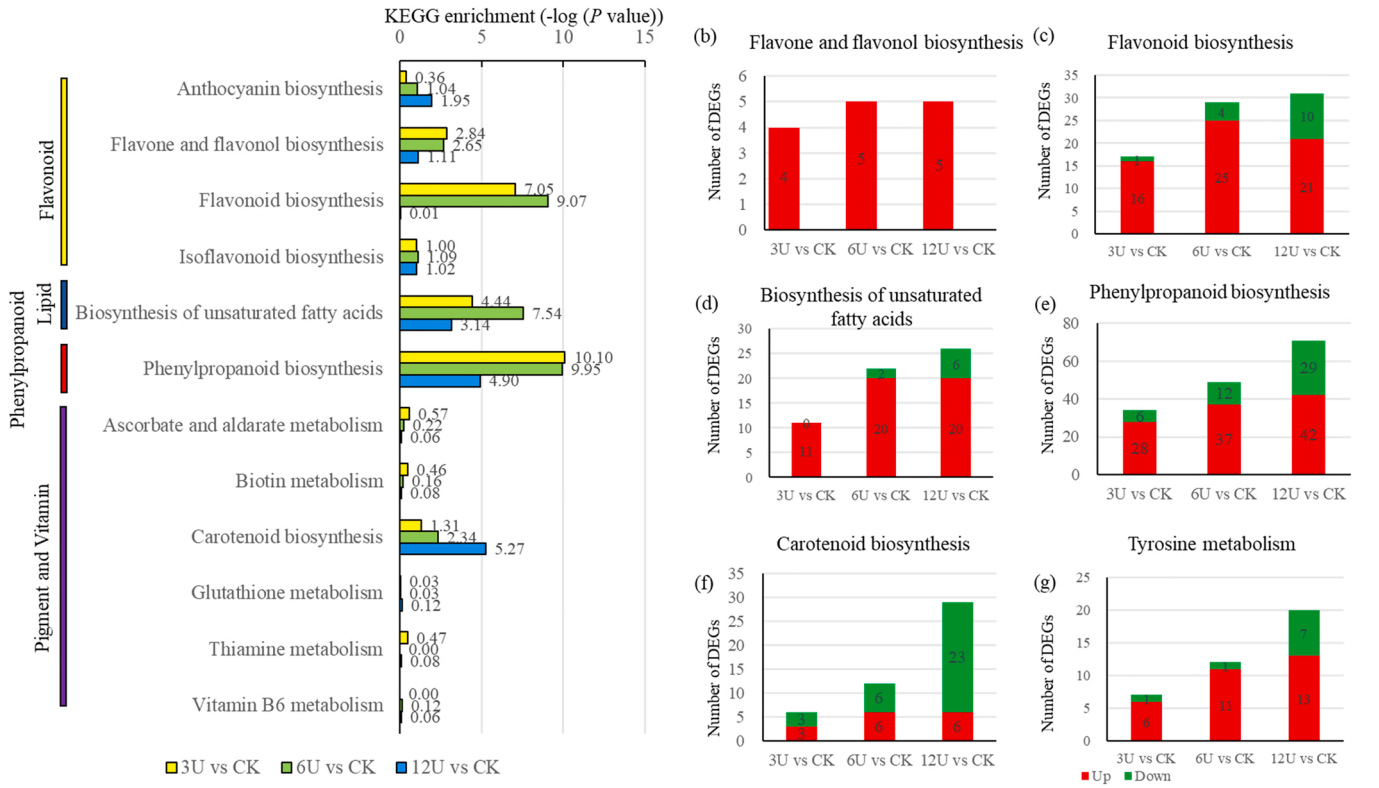

Fig. 3. Effects of UV-B treatment on primary and secondary metabolisms of *C. morifolium*. (a) KEGG enrichment analysis of DEGs related to primary and secondary metabolisms. The significant *P* value of each KEGG term in different comparisons are shown by a heatmap. All the KEGG terms were grouped into 11 metabolism-related categories, which were indicated by different color bars. Red boxes indicated the most significant enriched KEGG terms. The number of up- and down-regulated genes related to 'Flavone and flavonol biosynthesis' (b), 'Flavonoid biosynthesis' (c), 'Biosynthesis of unsaturated fatty acids' (d), 'Phenylpropanoid biosynthesis' (e), 'Carotenoid biosynthesis' (f), and 'Tyrosine metabolism' (g) terms.

term were significantly changed during the UV-B treatment process. For pigment metabolism, genes belonging to the "carotenoid biosynthesis" term were significantly changed at 12 h after UV-B exposure.

Notably, most DEGs related to flavonoid, unsaturated fatty acid, phenylpropanoid, and tyrosine metabolisms were induced by UV-B exposure. Only half of DEGs-related to carotenoid biosynthesis were induced by UV-B treatment at 3 h and 6 h, and most of the carotenoid biosynthesis-related genes were down-regulated at 12 h (Fig. 3b-g).

3.4. The effects of UV-B treatment on flavonoid and chlorogenic acid metabolism

Several flavonoid and chlorogenic acid biosynthesis-related DEGs were identified after UV-B radiation treatments. For precursor supply, eight phenylalanine ammonia-lyase (PAL) genes, two cinnamate 4-monooxygenase (C4M) genes, and eight 4-coumarate–CoA ligase (4CL) genes were identified as DEGs under UV-B radiation treatments. For flavonoid biosynthesis pathway, three chalcone synthase (CHS) genes, three chalcone–flavonone isomerase (CHI) genes, four flavanone 3-hydroxylase (F3H) genes, five flavonoid 3′-hydroxylase (F3′H) genes, one flavonol synthase (FLS) genes, five UDP-glucosyltransferase (UGT75) genes, two anthocyanidin synthase (ANS) genes, and one dihydroflavonol 4-reductase gene were identified as DEGs under UV-B radiation treatments. For chlorogenic acid biosynthesis pathway, 13 hydroxycinnamoyl CoA quinate transferase (HCT) genes, two hydroxycinnamoyl-CoA: quinate hydroxycinnamoyltransferase (HQT) genes, two p-coumarate 3-hydroxylase (C3H) genes, and three cinnamate beta-D-glucosyltransferase (UGCT) genes were identified as DEGs after UV-B radiation treatment (Fig. 4b).

3.5. Overview of miRNAomes

Four *C. morifolium* small RNA libraries exposed to UV-B radiation at different time points were constructed and sequenced (Table S5). Pearson correlation between different sample groups (three repeats for each group) were shown in Fig. S2. The length distribution of most reads was 18–25 bp in length (Fig. 5a). Small RNAs were classified into different groups, including rRNA, tRNA, snoRNA, snRNA, and other Rfam RNA. The rRNA group accounted for the largest proportion in samples (Fig. 5b). Venn diagram pointed out that five miRNAs were specifically detected in the CK group, 11 miRNAs were mainly detected in the UV 6 h group, 10 in the UV 12 h group, and four in the UV 3 h (Fig. 5c). Interestingly, 169 miRNAs were detected in all groups.

Based on their sequence features, miRNAs were classified into five groups: 1, 2a, 2b, 3, and 4. Group 4 miRNAs could not be mapped to selected pre-miRNAs in miRbase, and were thus considered novel miRNAs (Fig. 5d). *C. morifolium* miRNAs were classified into 38 typical families. The largest family was MIR156 (14 miRNAs), followed by MIR171_1 (11 miRNAs) and MIR414 families (nine miRNAs) (Fig. S3). Most detected miRNAs displayed high similarities to known miRNAs in other plants, such as 189 miRNAs were similar to miRNAs from *Glycine max* (Table S6).

3.6. Analysis of differentially expressed miRNAs (DEMs) after UV-B treatment

DEMs were identified after UV-B treatment (Fig. 6a). In total, 260 DEMs, including 22 DEMs in the UV 3 h/CK comparison, 15 DEMs in the UV 6 h/CK comparison, 21 DEMs in the UV 12 h/CK comparison, 25 DEMs in the UV 3 h/UV 6 h comparison, 22 DEMs in the UV 3 h/UV 12 h comparison, and 10 DEMs in the UV 6 h/UV 12 h comparison, were

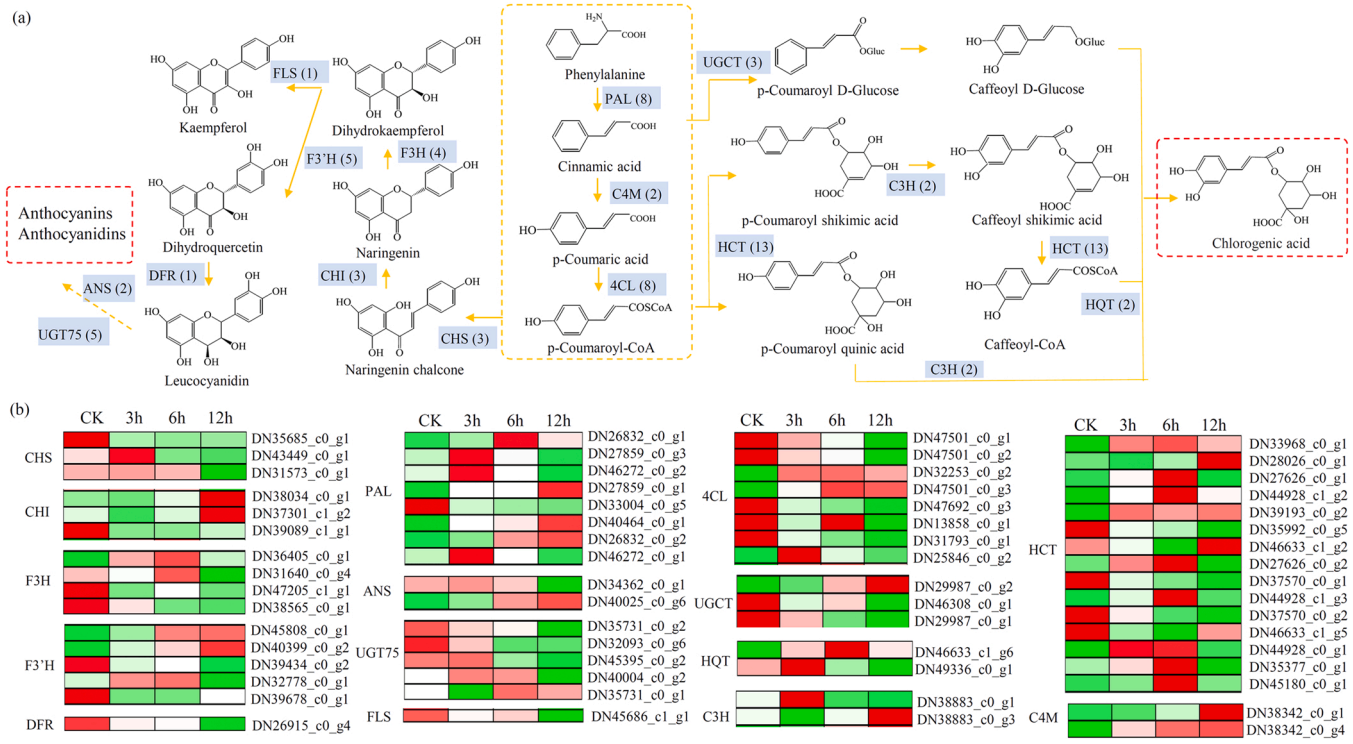

Fig. 4. Effects of UV-B treatment on flavonoid and chlorogenic acid metabolism. (a) Overview of flavonoid and chlorogenic acid metabolic pathway. Enzyme abbreviations: CHS: chalcone synthase; CHI: Chalcone–flavonone isomerase; F3H: flavanone 3-hydroxylase; F3′H: flavonoid 3′-monooxygenase; DFR: dihydroflavonol 4-reductase; FLS: flavonol synthase; UGT: UDP-glucosyltransferase; PAL: phenylalanine ammonia-lyase; ANS: anthocyanidin synthase; C4M: trans-cinnamate 4-monooxygenase; 4CL: 4-coumarate–CoA ligase; HCT: hydroxycinnamoyl CoA quinate transferase; HQT: hydroxycinnamoyl-CoA: quinate hydroxycinnamoyltransferase; and C3H: Coumaric acid-3-hydroxylase. (b) Expression changes of genes associated with flavonoid and chlorogenic acid metabolism under UV-B treatments in *C. morifolium*. The expression levels of each gene were normalized among four sample groups, including CK, 3 h, 6 h and 12 h. The red color indicated high expression level, green color indicated low expression level, and while color indicated median expression level. The heatmap scale ranges from − 1 to + 1 on a $\log_2$ scale normalized expression levels.

identified (Fig. 6b). UV-B responsive miRNAs were grouped into nine clusters, I to IX. Cluster IV, V, and VII contained most UV-B up-regulated miRNAs while Clusters III, VIII, and IX contained most UV-B down-regulated miRNAs. Interestingly, UV-B rapid responsive miRNAs belonged to Cluster I, while UV-B later responsive miRNAs belonged to Cluster VII (Fig. 6c).

3.7. Enrichment analysis of DEM targets

MiRNAs are implicated in many biological functions by regulating a series of downstream target genes. A total of 1954 unigenes were predicted to be targets of 118 miRNAs, including 36 novel miRNAs and 82 known miRNAs (Table S7).

GO enrichment analyses grouped most target genes into three main categories. In the 'biological process' group, significantly enriched GO terms comprised "regulation of transcription" ($P = 6.33E-14$) and "transcription" ($P = 3.32E-10$); in the 'cellular component' group, significantly enriched GO terms comprised the "nucleus" ($P = 7.11E-13$) and "SCF ubiquitin ligase complex" ($P = 1.19E-07$); and in the "molecular function" group, significantly enriched GO terms comprised "DNA-binding transcription factor activity" ($P = 2.22E-16$) and 'DNA binding' ($P = 1.62E-12$) (Table S8). The most significantly enriched KEGG terms were "plant hormone signal transduction" ($P = 2.32E-08$), and "ribosome biogenesis in eukaryotes" ($P = 4.11E-04$) terms (Fig. S4 and Table S9).

3.8. Flavonoid and chlorogenic acid metabolism-related gene-miRNA pairs

DEM targets contained five flavonoid and chlorogenic acid metabolism-related genes, including *4CL-like 9*, *4CL-like 5*, *CYP81E8*, *UGT91D1*, and *UGT72B1*. Specifically, *4CL-like 9* was a target of PC-5p-7136_1319, *4CL-like 5* was a target of PC-3p-78379_156, *CYP81E8* was a target of ath-MIR414-p5_2ss2CT21AC, and *UGT91D1* was a target of *PC-3p-154888_69*. Two target sites were identified in *UGT72B1* for *nta-miR171a_2ss8GT18GA* and *htu-miR403a* (Fig. 7a). *PC-5p-7136_1319* transcript levels were significantly up-regulated by UV-B radiation at U3 and U6 time points. The transcript of *PC-3p-78379_156* was largely induced by UV-B radiation at all time points. The expression of *ath-MIR414-p5_2ss2CT21AC* was significantly reduced at the later stage of UV-B radiation. *PC-3p-154888_69* and *htu-miR403a* transcript levels were induced at the early stage of UV-B radiation.

3.9. Flavonoid and chlorogenic acid metabolism-related TF-miRNA pairs

The MYB-bHLH complex was considered to play roles in the regulation of flavonoid and chlorogenic acid metabolism pathways (Xu et al., 2015). Among *C. morifolium* MYB genes, *CmMYB4* (DN32646) and *CmMYB12* (DN30067) were identified as targets of *ath-miR858a_L_1*, and *CmMYB44* (DN28492) was identified as a target of *PC-5p-79_56613* (Fig. 8a). The expression of *PC-5p-79_56613* was significantly up-regulated by UV-B radiation treatment at U6 time point (Fig. 8b). Among *C. morifolium* bHLH genes, *bHLH45* (DN46501) was the target of *ath-MIR414-p5_2ss15AC18AT* and *ath-MIR414-p5_2ss2CT21AC*. *BHLH62* (DN38440) was predicted to be the target of *aly-miR393a-5p* (Fig. 8c). The expression of *ath-MIR414-p5_2ss15AC18AT* was down-regulated at U3 but returned to normal levels at U6 and U12. The expression of ath-*MIR414-p5_2ss2CT21AC* was down-regulated at the later stage of UV-B radiation treatment (U6 and U12). In contrast, the transcript of *aly-mi393a-5p* was induced at the later stage of UV-B treatment (U6 and U12) (Fig. 8d).

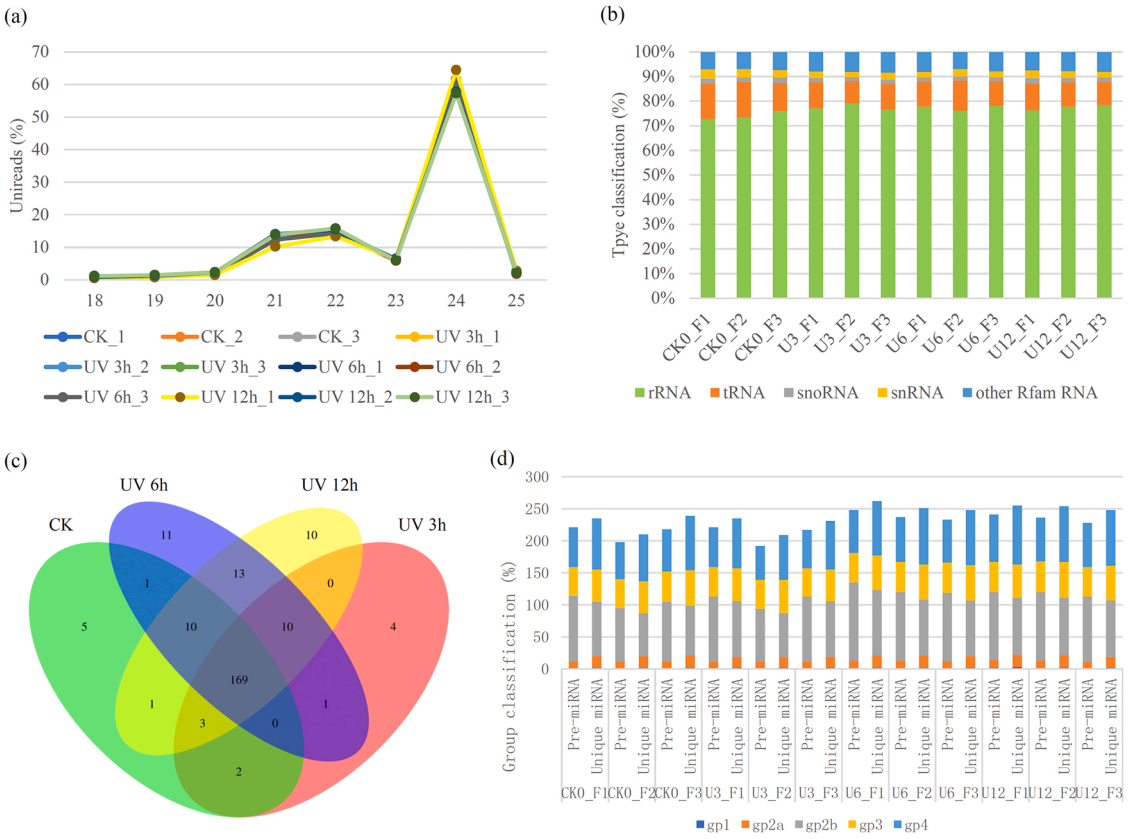

Fig. 5. Basic information for *C. morifolium* microRNAome. (a) Length distribution of all unique reads from four different groups. (b) Type classification of all sRNAs. The percentage of different RNA classes, including snRNA, snoRNA, tRNA, rRNA and other Rfam RNA, are shown in a histogram. (c) Venn diagrams of miRNAs expression overlap between UV-B treatment groups, including control, UV-B 3 h, UV-B 6 h, and UV-B 12 h. (d) Identification of known and novel miRNAs. All miRNAs were grouped into five groups, including gp1, gp2a, gp2b, gp3, and gp4, based on their sequence features. Gp1: Reads map to specific miRNAs/pre-miRNAs in miRbase and the pre-miRNAs further map to the reference sequence; gp2a: Reads map to selected miRNAs/pre-miRNAs in miRbase, and the mapped pre-miRNAs do not map to the reference sequence, but the reads map to the reference sequence; gp2b: Reads were mapped to miRNAs/pre-miRNAs of selected species in miRbase and the mapped pre-miRNAs were not further mapped to the reference sequence, but the reads were mapped to the reference sequence; gp3: Reads map to selected miRNAs/pre-miRNAs in miRbase, and the mapped pre-miRNAs do not map to the reference sequence, and the reads do not map to the reference sequence; and gp4: Reads do not map to selected pre-miRNAs in miRbase.

3.10. qRT-PCR confirmed mRNA and miRNA expression related to bioactive ingredient biosynthesis

The expression levels of eight key genes related to bioactive ingredient biosynthesis were analyzed using qRT-PCR. The expression levels of *MYB4*, *MYB44*, *CYP81E8* and *UGT91D1* were significantly increased, and *bHLH62*, *4CL-like 9*, and *UGT72B1* were significantly decreased under UV-B radiation treatments (Fig. S5). The expression levels of six key miRNAs related to bioactive ingredient biosynthesis were analyzed using stem-loop PCR. The expression levels of *PC-5p-7136_1319*, *PC-3p-78379_156*, *PC-5p-79_56613*, *ath-miR858a_L-1*, and *aly-miR393a-5p* were significantly increased under UV-B radiation treatments. The expression level of *ath-MIR414-p5_2ss2CT21AC* was significantly decreased under UV-B radiation treatments (Fig. S6). Expression levels of selected six miRNAs were basically consistent with the RNA sequencing data.

3.11. The target relationships between miRNA and mRNA

Dual-luciferase reporter system was used to confirm the predicted interaction between two randomly selected miRNAs and their targets. Our data suggested that *PC-3p-154888_69* and *PC-5p-79_56613* suppressed luciferase activity in WT-transfected cells, but not in mutant-transfected cells. *UGT91D1* is a target of *PC-3p-154888_69* and *MYB44* is a target of *PC-5p-79_56613* (Fig. S7).

4. Discussion

In China, medicinal *Chrysanthemum* has a long history and is an important export medicine. Moreover, tea made using *C. morifolium* inflorescences exerts multiple pharmacological and clinical effects, including anti-inflammatory, detoxification, eyesight improvement, and liver-heat removal qualities (Ma et al., 2022). Due to their economic value, active ingredient biosynthesis and regulation processes have been comprehensively investigated in-depth in different *Chrysanthemum* species (Chen et al., 2019a; Zhou et al., 2021b). We focused on *C. morifolium* inflorescences to identify regulatory mechanisms of active ingredient biosynthesis.

To date, several *C. morifolium* inflorescence transcriptomes have been published to reflect various development processes. For example, transcriptomic analyses provided new insights on petal senescence, ray floret morphogenesis, floral transition, and hooked petal morphogenesis (Ding et al., 2019; Pu et al., 2020; Ren et al., 2016; Yao et al., 2021). Transcriptomics analysis is used to screen environmental stimulus responsive genes. RNA-sequencing experiments identified 3858 hydroponic responsive genes, 5279 *Botrytis cinerea* attack responsive genes, and 2135 light-induced genes in *C. morifolium* (Ai et al., 2021; Kumar et al., 2020). In our study, thousands of UV-B responsive genes were identified in *C. morifolium* inflorescences, suggesting our analyses had sufficient sequencing depth to screen for valuable genes.

UV-B elicitor artificially induced flavonoid accumulation in plants

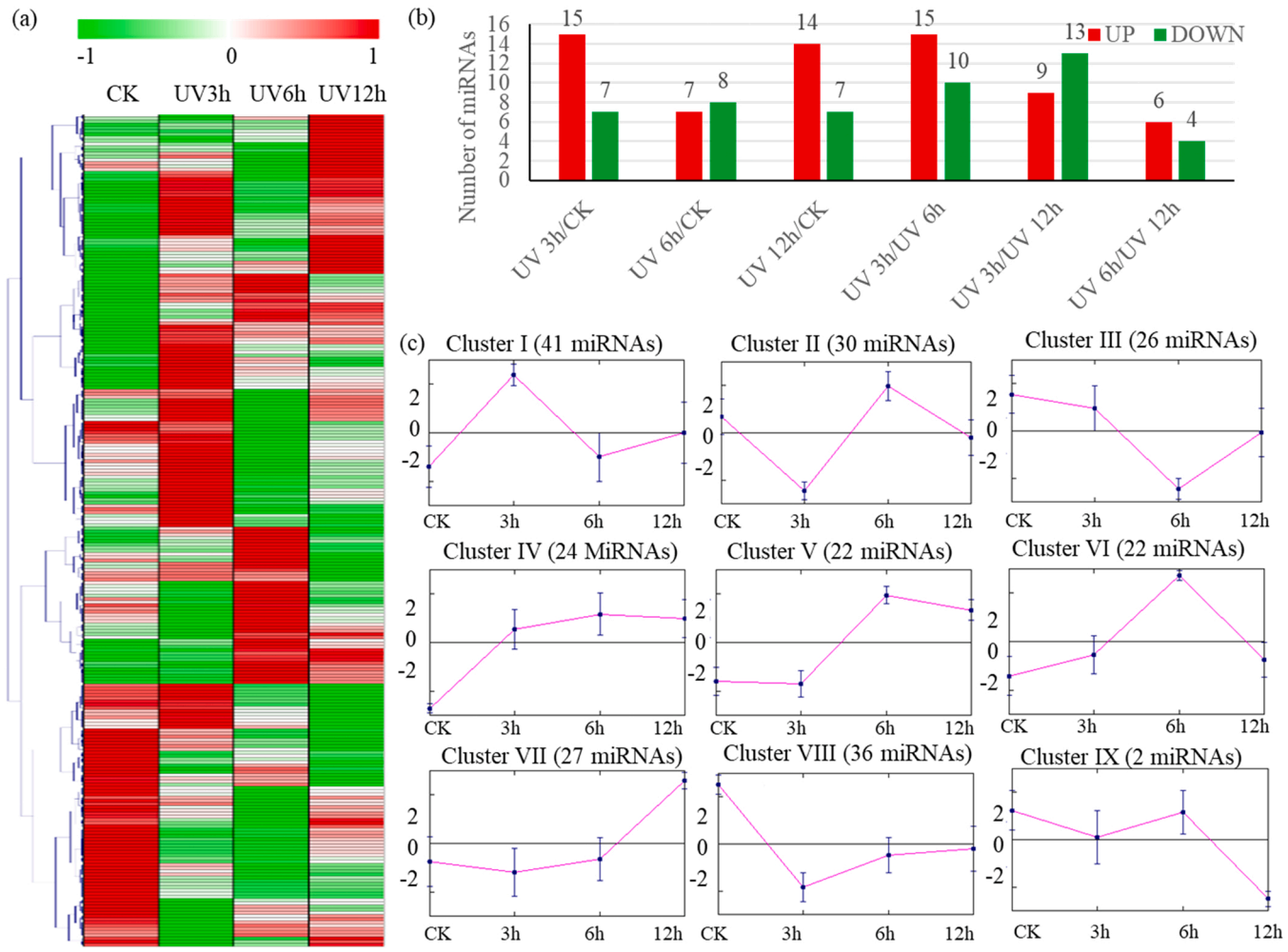

Fig. 6. Identification of UV-B responsive miRNAs in *C. morifolium.* (a) Heat map showing miRNAs expression pattern under different UV-B treatment conditions. (b) Number of up- and down-regulated miRNAs in different comparisons, including the UV 3 h vs CK, UV 6 h vs CK, UV12h vs CK, UV 3 h vs UV 6 h, UV 3 h vs UV 12 h, and UV 6 h vs UV 12 h. (c) MeV cluster analysis of differentially expressed miRNAs by the K-means method. All the identified miRNAs were grouped into nine Clusters. The heatmap scale ranges from − 1 to + 1 on a $\log_2$ scale.

where redox active flavonoids have evolved to prevent damages that is caused by UV-B radiation (Shi and Liu, 2021). In Qi and Huai *Chrysanthemum* inflorescences, UV-B radiation reportedly exerted significant effects active ingredient biosynthesis regulation (Yao et al., 2014). Chemical analysis pointed out that vitamin C, chlorogenic acid and flavones significantly accumulated in Qi *Chrysanthemum* inflorescences (Yao et al., 2015a). Enhanced UV-B treatment promoted various secondary metabolism pathways and facilitated active compound accumulation in post-harvest *Chrysanthemum* inflorescences (Si et al., 2015; Yao et al., 2015b). Our transcriptomic data showed that most DEGs were enriched in flavonoid, unsaturated fatty acid, phenylpropanoid, and carotenoid biosynthesis pathways (Fig. 3a). Expression analysis further confirmed that most DEGs were induced under UV-B treatments, suggesting a genetic basis for UV-B induced active ingredient biosynthesis.

Gene function analysis can help to reveal UV-B role in active component accumulation in *Chrysanthemum*. UV-B exposure significantly increased PLA and C4H enzyme activities in medicinal *Chrysanthemum* inflorescences (Ma et al., 2016). *C. morifolium* flavonoid and chlorogenic acid biosynthesis pathways were described in previous works (Yang et al., 2020, 2018). In a flavonoid and chlorogenic acid biosynthesis pathway, a number of UV-B responsive genes were identified, providing potential explanation for UV-B induced flavonoid and chlorogenic acid accumulation in *C. morifolium* inflorescences.

In *Chrysanthemum* plants, conserved miRNAs have various biological functions, including polyploidy breeding, embryo abortion, nitrogen starvation-responses, and salt and drought tolerance (Liu et al., 2021b; Song et al., 2015; Zhang et al., 2015; Zhang et al., 2017). Considerable evidence now suggests that plant miRNAs play roles in the responses of plant seedlings to various environmental signals by regulating the transcript levels of downstream target genes. In *C. indicum*, *miR396a* altered plant salt and drought tolerance by regulating two of its targets, *GRF1* and *GFR5* (Liu et al., 2021b). In *C. morifolium*, *miR160* and its targets, auxin response factors, were reportedly involved in normal embryo development (Zhang et al., 2017). In *C. nankingense*, *miR397* and its targets, *LAC* and *CL11869 ABC1-like* genes, were reported to be involved in nitrogen starvation responses (Song et al., 2015). In *C. dichrum*, *miR398* appeared to enhance freezing tolerance by regulating an *Inducer of CBF Expression* family gene (Chen et al., 2013). In our study, *4CL-like 5* and *9* were predicted as downstream targets of *PC-5p-7136_1319* and *PC-3p-78379_156*, respectively (Fig. 7a). 4CL-like proteins, which catalyze CoA ester formation, are key enzymes with important roles in flavonoid and lignin biosynthesis (Chen et al., 2019b). Interestingly, *UGT72B1*, a bifunctional O-glucosyltransferase encoding gene, was spliced by two miRNAs, *nta-miR171a_2ss8GT18GA* and *miR403a* (Brazier-Hicks et al., 2007). Our results suggested that several flavonoid and chlorogenic acid biosynthesis-related genes were regulated by UV-B induced miRNAs.

Several TFs, such as flavonoid metabolism-related MYB-bHLH-WDR

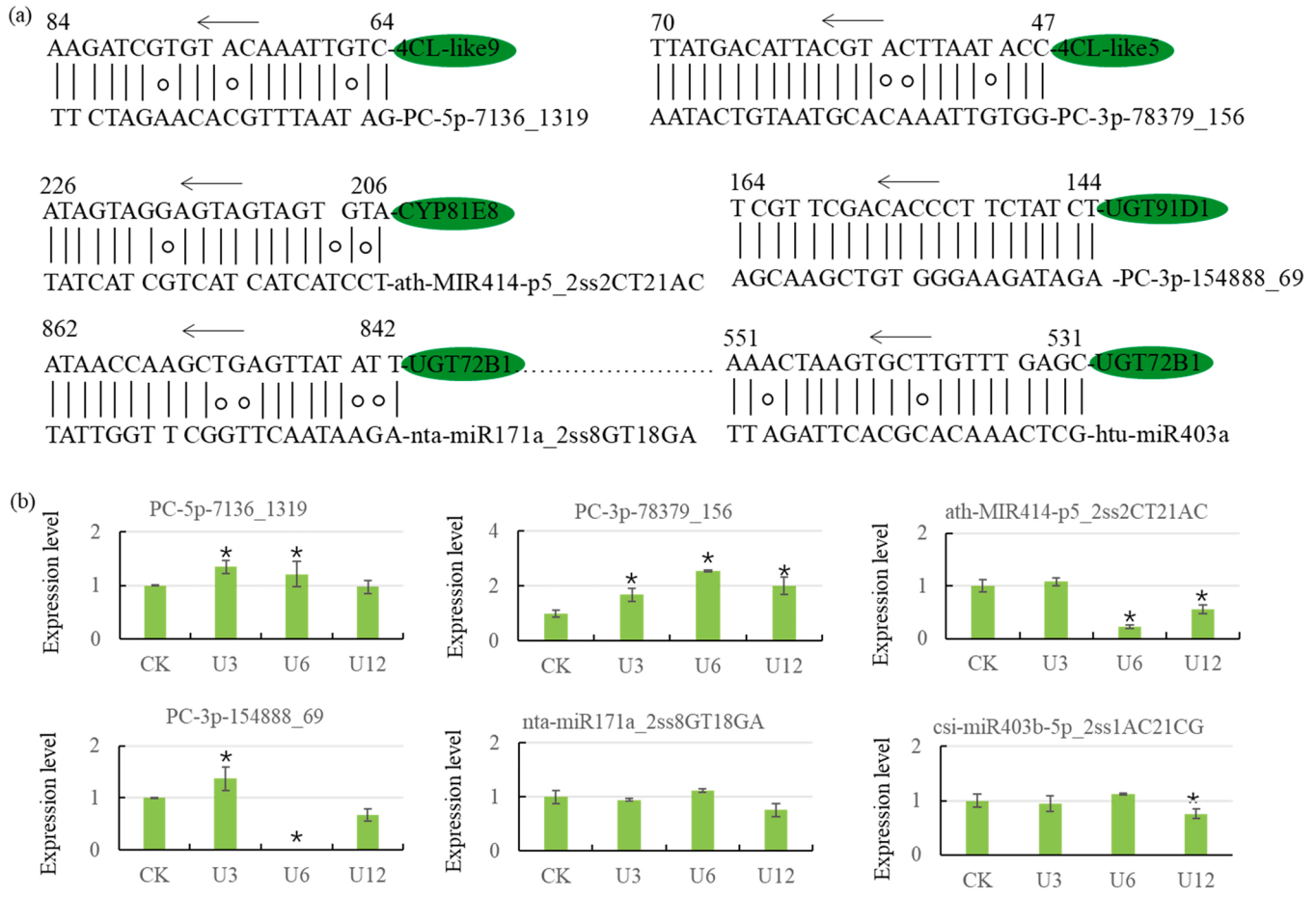

Fig. 7. Identification of flavonoid and chlorogenic acid metabolism-related gene-miRNAs. (a) Target genes were identified for PC-5p-7136_1319, PC-3p-78379_156, ath-MIR414-p5_2ss2CT21AC, PC-3p-154888_69, nta-miR171a_2ss8GT18GA, and csi-miR403b-5p_2ss1AC21CG. (b) Expression changes of miRNAs associated with flavonoid and chlorogenic acid metabolism genes under UV-B treatment in *Chrysanthemum*. "* " indicates a significant change ($P < 0.05$) in expression level between control and UV-B treatment. White circles indicated miss-matching pairs. Short vertical shoulders indicated matching pairs.

complex components, have been functionally characterized in many plants (Xu et al., 2015). Previous studies identified a series of MYB family genes, such as *CmMYB012*, *CmMYB21*, and *CmMYB7*, in *Chrysanthemum* (Wang et al., 2022; Xiang et al., 2019; Zhou et al., 2021a). In *C. morifolium* inflorescences, *miR858a_L-1* and its target gene, *CmMYB4* (DN32646), and *PC-5p-79_56613* and its target gene, *CmMYB44* (DN28492), were identified. In model plants, orthologous *CmMYB4/44* was reportedly involved in defense response (Yan et al., 2021). MiRNA-MYB pathway-mediated flavonoid accumulation may have important roles in *C. morifolium* inflorescence responses to UV-B treatment. Moreover, *ath-MIR414-p5_2ss15AC18AT/ath-MIR414-p5_2ss2CT21AC* and their target gene, *CmbHLH145* (DN46501), and *aly-miR393a-5p* and its target gene, *CmbHLH62* (DN38440), were identified. A recent study investigated how the activator complex CmMYB6-CmbHLH2 regulated petal anthocyanin homeostasis under different lights (Zhou et al., 2022). MiRNA-MYB pairs participate in a variety of biological processes, including growth, development, metabolism and other aspects. Our data suggested that miRNA-MYB pairs might play an essential role in regulation of flavonoid and chlorogenic acid biosynthesis.

In our study, UV-B responsive mRNAs and miRNAs in *C. morifolium* inflorescences were explored. Under UV-B radiation treatment, DEGs were enriched in flavonoid, unsaturated fatty acid, phenylpropanoid, and carotenoid biosynthesis pathways. Moreover, 169 miRNAs belonging to 38 typical families were detected. A total of 1954 unigenes were identified as target genes of 118 miRNAs. Six miRNAs were involved in active ingredient biosynthesis by regulating *4CL-like 5/9*, *CYP81E8*, *UGT91D1* and *UGT72B1*. Five miRNAs were involved in the transcriptional regulation of flavonoid biosynthesis by targeting *MYB4/44* and *bHLH45/62*. Our results provide a comprehensive resource for screening mRNAs and miRNAs implicated in the UV-B-mediated biosynthesis of bioactive ingredients in *C. morifolium* inflorescences.

Funding

This study was funded by the National Natural Science Foundation of China (Grant No. 82274038, 32271905, and 81803655), the Zhejiang Provincial Natural Science Foundation of China (Grant No. LY18H280012, LY19C150005, LY19C020003, and LY23C160001), Major Increase Or Decrease Program In The Central Finance Level (Grant No. 2060302), Zhejiang Provincial Key Research & Development Project Grants (Grant No. 2017C02011, 2018C02030).

CRediT authorship contribution statement

Yanjun Yang: Conceptualization, Data curation, Resources, Funding acquisition, Validation, Writing-original draft. **Jie Liu**: Data curation, Investigation, Software. **Taiyao Yi**: Data curation, Investigation, Software, Visualization. **Yao Li**: Formal analysis. **Mengyuan Li**: Software, Funding acquisition. **Haidi Liu:** Data curation, Resources, Investigation; Methodology. **Lijun Zheng:** Investigation; Methodology, Writing-original draft. **Zhehao Chen:** Data curation, Resources, Supervision, Visualization. **Juan Hao:** Data curation, Resources, Supervision, Visualization. **Maojun Xu:** Conceptualization, Funding acquisition, Project administration, Writing - review & editing. **Chenjia Shen:**

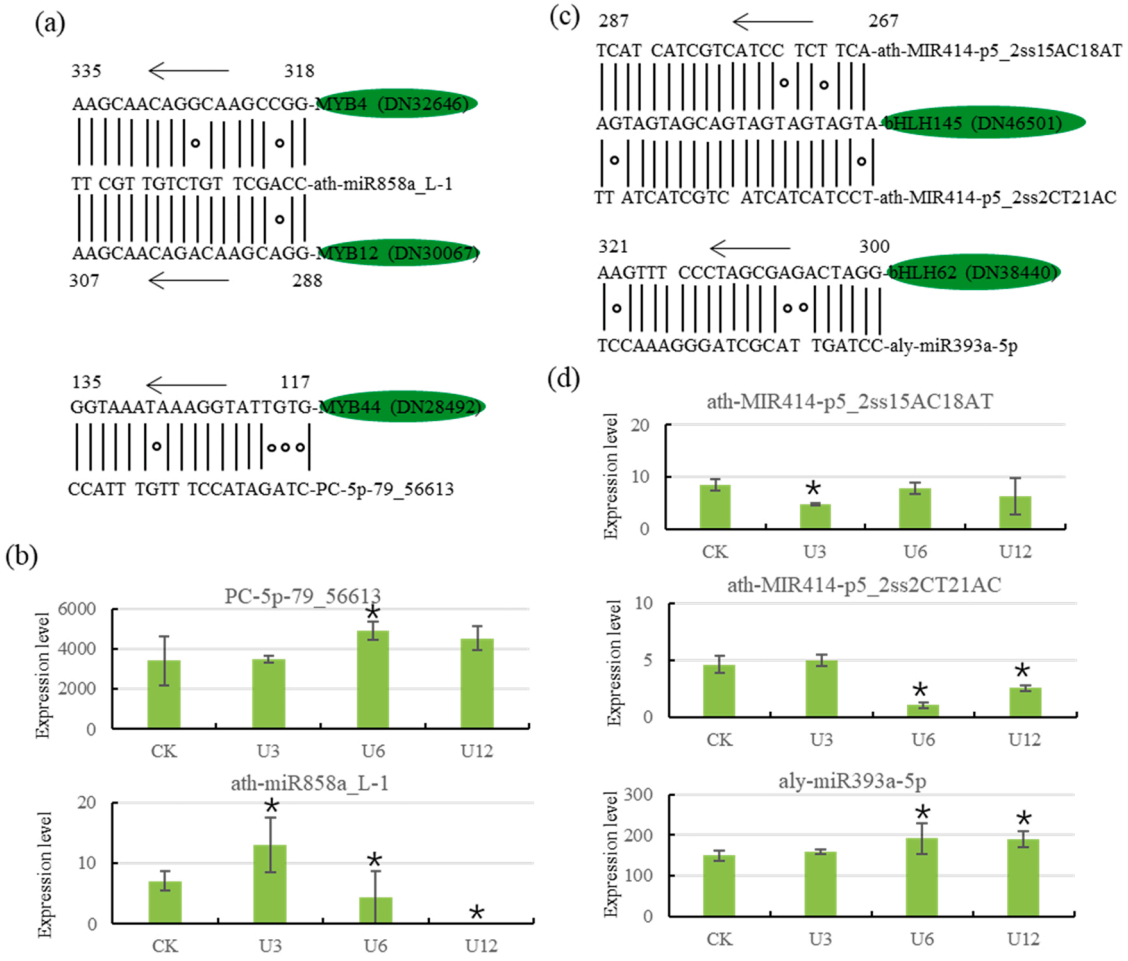

Fig. 8. Identification of flavonoid and chlorogenic acid metabolism-related TFs-miRNAs. (a) MYB family members and their potential target miRNAs. (b) Expression changes of miRNAs associated with MYBs under UV-B treatment in *Chrysanthemum*. "* " indicates significant a change ($P < 0.05$) in expression level between control and UV-B treatment. (c) bHLH family members and their potential target miRNAs. (d) Expression changes of miRNAs associated with bHLHs under UV-B treatment in *Chrysanthemum*. "*" indicates a significant change ($P < 0.05$) in expression level between control and UV-B treatment. White circles indicated miss-matching pairs. Short vertical shoulders indicated matching pairs.

Conceptualization, Writing - review & editing.

Declaration of Competing Interest

The authors declare that they have no known competing financial interests or personal relationships that could have appeared to influence the work reported in this paper.

Data availability

Data will be made available on request.

Appendix A. Supporting information

Supplementary data associated with this article can be found in the online version at doi:10.1016/j.indcrop.2023.116657.

References

Ai, P., Liu, X., Li, Z., Kang, D., Khan, M.A., Li, H., Shi, M., Wang, Z., 2021. Comparison of chrysanthemum flowers grown under hydroponic and soil-based systems: yield and transcriptome analysis. BMC Plant Biol. 21, 517.

Anderson, N.O., 2006. Flower breeding and genetics / issues, challenges and opportunities for the 21st century.

Brazier-Hicks, M., Offen, W.A., Gershater, M.C., Revett, T.J., Lim, E.K., Bowles, D.J., Davies, G.J., Edwards, R., 2007. Characterization and engineering of the bifunctional N- and O-glucosyltransferase involved in xenobiotic metabolism in plants. Proc. Natl. Acad. Sci. USA 104, 20238–20243.

Chen, M., Wang, K., Zhang, Y., Zhang, M., Ma, Y., Sun, H., Jin, Z., Zheng, H., Jiang, H., Yu, P., Zhang, Y., Sun, H., 2019a. New insights into the biological activities of Chrysanthemum morifolium: Natural flavonoids alleviate diabetes by targeting alpha-glucosidase and the PTP-1B signaling pathway. Eur. J. Med. Chem. 178, 108–115.

Chen, X., Wang, H., Li, X., Ma, K., Zhan, Y., Zeng, F., 2019b. Molecular cloning and functional analysis of 4-Coumarate:CoA ligase 4(4CL-like 1)from Fraxinus mandshurica and its role in abiotic stress tolerance and cell wall synthesis. BMC Plant Biol. 19, 231.

Chen, Y., Jiang, J., Song, A., Chen, S., Shan, H., Luo, H., Gu, C., Sun, J., Zhu, L., Fang, W., Chen, F., 2013. Ambient temperature enhanced freezing tolerance of Chrysanthemum dichrum CdICE1 Arabidopsis via miR398. BMC Biol. 11, 121.

Chen, Y., Shen, Q., Lv, P., Sun, C., 2020. Comparative metabolomic analyses of Dendrobium officinale Kimura et Migo responding to UV-B radiation reveal variations in the metabolisms associated with its bioactive ingredients. PeerJ 8, e9107.

Ding, L., Zhao, K., Zhang, X., Song, A., Su, J., Hu, Y., Zhao, W., Jiang, J., Chen, F., 2019. Comprehensive characterization of a floral mutant reveals the mechanism of hooked petal morphogenesis in Chrysanthemum morifolium. Plant Biotechnol. J. 17, 2325–2340.

Dong, Q., Hu, B., Zhang, C., 2022. microRNAs and their roles in plant development. Front. Plant Sci. 13, 824240.

Feng, S., Kailin, H., Zhang, H., Chen, C., Huang, J., Wu, Q., Zhang, Z., Gao, Y., Wu, X., Wang, H., Shen, C., 2023. Investigation of the role of TmMYB16/123 and their targets (TmMTP1/11) in the tolerance of Taxus media to cadmium. Tree Physiol.

Hao, J., Lou, P., Han, Y., Zheng, L., Lu, J., Chen, Z., Ni, J., Yang, Y., Xu, M., 2022. Ultraviolet-B irradiation increases antioxidant capacity of Pakchoi (Brassica rapa L.) by inducing flavonoid biosynthesis. Plants 11.

Haunsberger, S.J., Connolly, N.M., Prehn, J.H., 2017. miRNAmeConverter: an R/bioconductor package for translating mature miRNA names to different miRBase versions. Bioinformatics 33, 592–593.
Hong, Y., Tang, X., Huang, H., Zhang, Y., Dai, S., 2015. Transcriptomic analyses reveal species-specific light-induced anthocyanin biosynthesis in chrysanthemum. BMC Genom. 16, 202.
Jaiswal, D., Pandey, A., Agrawal, M., Agrawal, S.B., 2022. Photosynthetic, biochemical and secondary metabolite changes in a medicinal plant chlorophytum borivillianum (Safed musli) against low and high doses of UV-B radiation. Photochem. Photobiol.
Jo, Y.D., Ryu, J., Kim, Y.S., Kang, K.Y., Hong, M.J., Choi, H.I., Lim, G.H., Kim, J.B., Kim, S.H., 2020. Dramatic increase in content of diverse flavonoids accompanied with down-regulation of F-box genes in a chrysanthemum (Chrysanthemum x morifolium (Ramat.) Hemsl.) mutant cultivar producing dark-purple ray florets. Genes 11.
Kazeroonian, R., Mousavi, A., Jari, S.K., Tohidfar, M., 2018. Factors influencing in vitro organogenesis of chrysanthemum morifolium cv. 'resomee splendid'. Iran. J. Biotechnol. 16, e1454.
Kumar, V., Hatan, E., Bar, E., Davidovich-Rikanati, R., Doron-Faigenboim, A., Spitzer-Rimon, B., Elad, Y., Alkan, N., Lewinsohn, E., Oren-Shamir, M., 2020. Phenylalanine increases chrysanthemum flower immunity against Botrytis cinerea attack. Plant J.: Cell Mol. Biol. 104, 226–240.
Li, Y., Kong, D., Fu, Y., Sussman, M.R., Wu, H., 2020. The effect of developmental and environmental factors on secondary metabolites in medicinal plants. Plant Physiol. Biochem. 148, 80–89.
Liu, H., Luo, C., Chen, D., Wang, Y., Guo, S., Chen, X., Bai, J., Li, M., Huang, X., Cheng, X., Huang, C., 2021a. Whole-transcriptome analysis of differentially expressed genes in the mutant and normal capitula of Chrysanthemum morifolium. BMC Genom. Data 22, 2.
Liu, X., Xia, B., Purente, N., Chen, B., Zhou, Y., He, M., 2021b. Transgenic Chrysanthemum indicum overexpressing cin-miR396a exhibits altered plant development and reduced salt and drought tolerance. Plant Physiol. Biochem. 168, 17–26.
Lu, B., Li, M., Yin, R., 2016. Phytochemical content, health benefits, and toxicology of common edible flowers: a review (2000-2015). Crit. Rev. Food Sci. Nutr. 56 (Suppl 1). S130-148.
Lu, C., Pu, Y., Liu, Y., Li, Y., Qu, J., Huang, H., Dai, S., 2019. Comparative transcriptomics and weighted gene co-expression correlation network analysis (WGCNA) reveal potential regulation mechanism of carotenoid accumulation in Chrysanthemum x morifolium. Plant Physiol. Biochem. 142, 415–428.
Ma, A., Zou, F., Zhang, R., Zhao, X., 2022. The effects and underlying mechanisms of medicine and food homologous flowers on the prevention and treatment of related diseases. J. Food Biochem., e14430
Ma, C.H., Chu, J.Z., Shi, X.F., Liu, C.Q., Yao, X.Q., 2016. Effects of enhanced UV-B radiation on the nutritional and active ingredient contents during the floral development of medicinal chrysanthemum. J. Photochem. Photobiol. B 158, 228–234.
Manivannan, A., Soundararajan, P., Park, Y.G., Jeong, B.R., 2016. Chemical elicitor-induced modulation of antioxidant metabolism and enhancement of secondary metabolite accumulation in cell suspension cultures of scrophularia kakudensis Franch. Int. J. Mol. Sci. 17, 399.
Pandey, A., Jaiswal, D., Agrawal, S.B., 2021. Ultraviolet-B mediated biochemical and metabolic responses of a medicinal plant Adhatoda vasica Nees. at different growth stages. J. Photochem. Photobiol. B 216, 112142.
Pu, Y., Huang, H., Wen, X., Lu, C., Zhang, B., Gu, X., Qi, S., Fan, G., Wang, W., Dai, S., 2020. Comprehensive transcriptomic analysis provides new insights into the mechanism of ray floret morphogenesis in chrysanthemum. BMC Genom. 21, 728.
Ren, L., Liu, T., Cheng, Y., Sun, J., Gao, J., Dong, B., Chen, S., Chen, F., Jiang, J., 2016. Transcriptomic analysis of differentially expressed genes in the floral transition of the summer flowering chrysanthemum. BMC Genom. 17, 673.
Sablok, G., Yang, K., Wen, X., 2019. Protocols for miRNA target prediction in plants. Methods Mol. Biol. 1970, 65–73.
Shi, C., Liu, H., 2021. How plants protect themselves from ultraviolet-B radiation stress. Plant Physiol. 187, 1096–1103.
Si, C., Yao, X.Q., He, X.L., Chu, J.Z., Ma, C.H., Shi, X.F., 2015. Effects of enhanced UV-B radiation on biochemical traits in postharvest flowers of medicinal chrysanthemum. Photochem. Photobiol. 91, 845–850.
Song, A., Wang, L., Chen, S., Jiang, J., Guan, Z., Li, P., Chen, F., 2015. Identification of nitrogen starvation-responsive microRNAs in Chrysanthemum nankingense. Plant Physiol. Biochem. 91, 41–48.
Song, A., Gao, T., Li, P., Chen, S., Guan, Z., Wu, D., Xin, J., Fan, Q., Zhao, K., Chen, F., 2016a. Transcriptome-wide identification and expression profiling of the DOF transcription factor gene family in chrysanthemum morifolium. Front. Plant Sci. 7, 199.
Song, A., Gao, T., Wu, D., Xin, J., Chen, S., Guan, Z., Wang, H., Jin, L., Chen, F., 2016b. Transcriptome-wide identification and expression analysis of chrysanthemum SBP-like transcription factors. Plant Physiol. Biochem. 102, 10–16.
Song, A., Li, P., Xin, J., Chen, S., Zhao, K., Wu, D., Fan, Q., Gao, T., Chen, F., Guan, Z., 2016c. Transcriptome-wide survey and expression profile analysis of putative chrysanthemum HD-Zip I and II genes. Genes 7.
Song, A., Wu, D., Fan, Q., Tian, C., Chen, S., Guan, Z., Xin, J., Zhao, K., Chen, F., 2016d. Transcriptome-wide identification and expression profiling analysis of chrysanthemum trihelix transcription factors. Int. J. Mol. Sci. 17.
Su, J., Jiang, J., Zhang, F., Liu, Y., Ding, L., Chen, S., Chen, F., 2019. Current achievements and future prospects in the genetic breeding of chrysanthemum: a review. Hortic. Res. 6, 109.
Takshak, S., Agrawal, S.B., 2016. The role of supplemental ultraviolet-B radiation in altering the metabolite profile, essential oil content and composition, and free radical scavenging activities of Coleus forskohlii, an indigenous medicinal plant. Environ. Sci. Pollut. Res. Int. 23, 7324–7337.
Teixeira da Silva, J.A., 2003. Chrysanthemum: advances in tissue culture, cryopreservation, postharvest technology, genetics and transgenic biotechnology. Biotechnol. Adv. 21, 715–766.
Wang, Y., Zhou, L.J., Wang, Y., Geng, Z., Ding, B., Jiang, J., Chen, S., Chen, F., 2022. An R2R3-MYB transcription factor CmMYB21 represses anthocyanin biosynthesis in color fading petals of chrysanthemum. Sci. Hortic. 293, 110674.
Xia, X., Shao, Y., Jiang, J., Du, X., Sheng, L., Chen, F., Fang, W., Guan, Z., Chen, S., 2015. MicroRNA expression profile during aphid feeding in chrysanthemum (Chrysanthemum morifolium). PLOS One 10, e0143720.
Xiang, L., Liu, X., Li, H., Yin, X., Grierson, D., Li, F., Chen, K., 2019. CmMYB#7, an R3 MYB transcription factor, acts as a negative regulator of anthocyanin biosynthesis in chrysanthemum. J. Exp. Bot.
Xu, M., Jiang, Y., Chen, S., Chen, F., Chen, F., 2021. Herbivory-induced emission of volatile terpenes in chrysanthemum morifolium functions as an indirect defense against spodoptera litura larvae by attracting natural enemies. J. Agric. Food Chem. 69, 9743–9753.
Xu, W., Dubos, C., Lepiniec, L., 2015. Transcriptional control of flavonoid biosynthesis by MYB-bHLH-WDR complexes. Trends Plant Sci. 20, 176–185.
Yan, X., Huang, Y., Song, H., Chen, F., Geng, Q., Hu, M., Zhang, C., Wu, X., Fan, T., Cao, S., 2021. A MYB4-MAN3-Mannose-MNB1 signaling cascade regulates cadmium tolerance in Arabidopsis. PLOS Genet/ 17, e1009636.
Yang, Y., Jiang, Z., Guo, J., Yang, X., Xu, N., Chen, Z., Hao, J., Li, J., Pang, J., Shen, C., Xu, M., 2018. Transcriptomic analyses of Chrysanthemum morifolium Ramat under UV-B radiation treatment reveal variations in the metabolisms associated with bioactive components. Ind. Crops Prod. 124, 475–486.
Yang, Y., Guo, J., Cheng, J., Jiang, Z., Xu, M., 2020. Identification of UV-B radiation responsive microRNAs and their target genes in chrysanthemum (Chrysanthemum morifolium Ramat) using high-throughput sequencing. Ind. Crops Prod. 151, 112484.
Yao, J., Li, R., Cheng, Y., Li, Z., 2021. A combined transcriptomic and proteomic analysis of chrysanthemum provides new insights into petal senescence. Planta 255, 22.
Yao, X., Jianzhou, C., Xueli, H., Binbin, L., Jingmin, L., Zhaowei, Y., 2013. Effects of selenium on agronomical characters of winter wheat exposed to enhanced ultraviolet-B. Ecotoxicol. Environ. Saf. 92, 320–326.
Yao, X., Chu, J., He, X., Ma, C., Han, C., Shen, H., 2015a. The changes in quality ingredients of Qi chrysanthemum flowers treated with elevated UV-B radiation at different growth stages. J. Photochem. Photobiol. B 146, 18–23.
Yao, X., Chu, J.Z., Ma, C.H., Si, C., Li, J.G., Shi, X.F., Liu, C.N., 2015b. Biochemical traits and proteomic changes in postharvest flowers of medicinal chrysanthemum exposed to enhanced UV-B radiation. J. Photochem. Photobiol. B 149, 272–279.
Yao, X.Q., Chu, J.Z., He, X.L., Si, C., 2014. The effects of UV-B radiation intensity on biochemical parameters and active ingredients in flowers of Qi chrysanthemum and Huai chrysanthemum. Photochem. Photobiol. 90, 1308–1313.
Yuan, H., Jiang, S., Liu, Y., Daniyal, M., Jian, Y., Peng, C., Shen, J., Liu, S., Wang, W., 2020. The flower head of Chrysanthemum morifolium Ramat. (Juhua): a paradigm of flowers serving as Chinese dietary herbal medicine. J. Ethnopharmacol. 261, 113043.
Zhan, X., Chen, Z., Chen, R., Shen, C., 2022. Environmental and genetic factors involved in plant protection-associated secondary metabolite biosynthesis pathways. Front. Plant Sci. 13, 877304.
Zhang, F., Dong, W., Huang, L., Song, A., Wang, H., Fang, W., Chen, F., Teng, N., 2015. Identification of MicroRNAs and their targets associated with embryo abortion during chrysanthemum cross breeding via high-throughput sequencing. PLOS One 10, e0124371.
Zhang, F., Zhao, J., Xu, S., Fang, W., Chen, F., Teng, N., 2017. MicroRNA and putative target discoveries in chrysanthemum polyploidy breeding. Int. J. Genom. 2017, 6790478.
Zhang, W., Jiang, Y., Chen, F., Guan, Z., Wei, G., Chen, X., Zhang, C., Kollner, T.G., Chen, S., Chen, F., Chen, F., 2022. Dynamic regulation of volatile terpenoid production and emission from Chrysanthemum morifolium capitula. Plant Physiol. Biochem. 182, 11–21.
Zheng, H., Yu, M.Y., Han, Y., Tai, B., Ni, S.F., Ji, R.F., Pu, C.J., Chen, K., Li, F.Q., Xiao, H., Shen, Y., Zhou, X.T., Huang, L.Q., 2022. Comparative transcriptomics and metabolites analysis of two closely related euphorbia species reveal environmental adaptation mechanism and active ingredients difference. Front. Plant Sci. 13, 905275.
Zhou, L.J., Geng, Z., Wang, Y., Wang, Y., Liu, S., Chen, C., Song, A., Jiang, J., Chen, S., Chen, F., 2021a. A novel transcription factor CmMYB012 inhibits flavone and anthocyanin biosynthesis in response to high temperatures in chrysanthemum. Hortic. Res. 8, 248.
Zhou, L.J., Wang, Y., Wang, Y., Song, A., Jiang, J., Chen, S., Ding, B., Guan, Z., Chen, F., 2022. Transcription factor CmbHLH16 regulates petal anthocyanin homeostasis under different lights in Chrysanthemum. Plant Physiol. 190, 1134–1152.
Zhou, Z., Xian, J., Wei, W., Xu, C., Yang, J., Zhan, R., Ma, D., 2021b. Volatile metabolic profiling and functional characterization of four terpene synthases reveal terpenoid diversity in different tissues of Chrysanthemum indicum L. Phytochemistry 185, 112687.